

OPEN ACCESS

Polymer-in-Ceramic Nanocomposite Solid Electrolyte for Lithium Metal Batteries Encompassing PEO-Grafted TiO₂ Nanocrystals

To cite this article: Francesco Colombo *et al* 2020 *J. Electrochem. Soc.* **167** 070535

View the [article online](#) for updates and enhancements.



PRIMETM
PACIFIC RIM MEETING
ON ELECTROCHEMICAL
AND SOLID STATE SCIENCE
2020

Abstract Submission
DEADLINE EXTENDED:
May 1, 2020



Honolulu, HI | October 4-9, 2020







Polymer-in-Ceramic Nanocomposite Solid Electrolyte for Lithium Metal Batteries Encompassing PEO-Grafted TiO₂ Nanocrystals

Francesco Colombo,¹ Simone Bonizzoni,¹ Chiara Ferrara,¹ Roberto Simonutti,¹ Michele Mauri,¹  Marisa Falco,² Claudio Gerbaldi,² Piercarlo Mustarelli,^{1,z}  and Riccardo Ruffo¹

¹Department of Materials Science, University of Milano-Bicocca, and INSTM, 20125 Milano, Italy

²GAME Lab, Department of Applied Science and Technology (DISAT), Politecnico di Torino, 10129 Torino, Italy

Lithium Metal Batteries (LMB) require solid or quasi-solid electrolytes able to block dendrites formation during cell cycling. Polymer-in-ceramic nanocomposites with the ceramic fraction exceeding the one normally used as the filler ($>10 \div 15$ wt%) are among the most interesting options on the table. Here, we report on a new hybrid material encompassing brush-like TiO₂ nanocrystals functionalized with low molecular weight poly(ethylene oxide) (PEO). The nanocomposite electrolyte membranes are then obtained by blending the brush-like nanocrystals with high molecular weight PEO and LiTFSI. The intrinsic chemical compatibility among the PEO moieties allows a TiO₂ content as high as ~ 39 wt% (90:10 w/w functionalized nanocrystals/PEO-LiTFSI), while maintaining good processability and mechanical resistance. The 50:50 w/w nanocomposite electrolyte (18.8 wt% functionalized TiO₂) displays ionic conductivity of 3×10^{-4} S cm⁻¹ at 70 °C. Stripping/plating experiments show an excellent long-term behavior even at relatively high currents of 200 μ A cm⁻². Upon testing in a lab-scale Li/electrolyte/LiFePO₄ cell, the material delivers 130 mAh g⁻¹ and 120 mAh g⁻¹ after 40 and 50 cycles at 0.05 and 0.1 mA, respectively, with Coulombic efficiency exceeding 99.5%, which demonstrates the very promising prospects of these newly developed nanocomposite solid electrolyte for future development of LMBs.

© 2020 The Author(s). Published on behalf of The Electrochemical Society by IOP Publishing Limited. This is an open access article distributed under the terms of the Creative Commons Attribution 4.0 License (CC BY, <http://creativecommons.org/licenses/by/4.0/>), which permits unrestricted reuse of the work in any medium, provided the original work is properly cited. [DOI: 10.1149/1945-7111/ab7c72]



Manuscript submitted January 14, 2020; revised manuscript received February 17, 2020. Published March 13, 2020. *This paper is part of the JES Focus Issue on Challenges in Novel Electrolytes, Organic Materials, and Innovative Chemistries for Batteries in Honor of Michel Armand.*

Supplementary material for this article is available [online](#)

In the next future, also thanks to full exploitation of nanotechnology, lithium batteries are expected to play a main role not only in powering small electronic equipment, but also to feed more demanding sectors such as automotive and massive grid storage.¹ However, this paradigmatic change will hardly be obtained through incremental optimization of present Li-ion battery (LIB) systems, e. g. simply by making the step from so-called generation 2 to 3 following EU Set-plan.² In contrast, substituting graphite (or even C/Si composite) anode with lithium metal, coupled with a suitable truly solid-state electrolyte may open the way towards the exploitation of high energy density batteries, and even of alternative chemistries (e. g. Li/S, Li/air).^{3,4}

The development of lithium metal batteries (LMB) imposes further and more rigid constraints on the electrolyte design with respect to conventional LIBs.⁵ In fact, in addition to the well-known requirements for today's liquid electrolytes, which include high conductivity, chemical and electrochemical stability against the electrodes, low flammability, and environmental sustainability,⁶ the electrolytes for LMBs must also be able to block the formation of lithium dendrites, e.g. by forming stable solid electrolyte interface (SEI) onto the metal anode, and/or by constituting by themselves a high-elastic-modulus barrier.^{7,8}

To this aim, solid electrolytes, including ceramics and polymer-ceramic hybrids, with or without lithium salts, have been proposed in the recent years.⁹⁻¹² Polymer-ceramic composites where the polymeric fraction is constituted by poly(ethylene oxide) (PEO) and a lithium salt were widely studied during the last 25 years.¹³ In particular, the ceramic phase was there intended as a nano-scale filler accounting 5–15 wt% of the polymer-salt content ("ceramic-in-polymer" region of the phase diagram). The main functional advantage of the filler addition was a conductivity increase up to about one order of magnitude with respect to the polymer-salt corresponding composition. More recently, the attention has been

focused on hybrid ceramic-polymer electrolyte membranes composed of inorganic solid Li-ion electrolytes and Li-conducting polymers, which may offer enhanced ionic mobility, good mechanical properties and room temperature processing.¹⁴⁻¹⁷ Also in this case, however, most of the abovementioned studies have been focused to the ceramic-in-polymer region, chiefly because of the easier film processability. Nonetheless, the innovative approach related to the preparation of "polymer-in-ceramic" electrolytes, with the presence of a predominant ceramic component (> 50 %), is growing in importance and is regarded as an effective way to advance the development of all solid-state batteries.^{18,19} Due to the high mechanical strength and safety pertaining to such hybrid membranes, they are considered appropriate for big battery packs used in electric vehicles.¹⁵ The main drawbacks of polymer-in-ceramic hybrids are indeed related to the low chemical and mechanical compatibilities between the ceramic phase and the polymeric one, which lead to bad processability and/or properties degradation upon prolonged cycling.

In this paper we report on a novel polymer-in-ceramic nanocomposite solid electrolyte, where the ceramic phase is constituted by TiO₂ nanocrystals grafted with low molecular weight (MW = 5000) poly(ethylene oxide) (PEO_{5K}) moieties. Free-standing films are obtained by dispersing the ceramic phase in high molecular weight (MW = 4000000) PEO (PEO_{4M}) in which LiTFSI is dissolved. The chemical compatibility between PEO_{5K} and PEO_{4M} allows obtaining excellent film-forming properties up to ~ 39 wt% TiO₂, resulting in enhanced transport and electrochemical properties of the resulting nanocomposite solid-state electrolyte.

Experimental

Raw materials.—Poly(ethylene oxide), MW = 4000000 (PEO_{4M}) was bought from BDH Chemicals. Poly(ethylene oxide) methyl ether, MW = 5000 (PEO_{5K}), titanium tetraisopropoxide (TTIP), trimethylamine N-oxide (TMAO), phosphoryl chloride (POCl₃), triethylamine (TEA), bis(trifluoromethanesulfonyl)imide

^zE-mail: piercarlo.mustarelli@unimib.it

(LiTFSI), N-Methyl-2-pyrrolidone (NMP), chloroform, acetonitrile, dimethyl carbonate (DMC), n-hexane and diethyl ether were purchased from Sigma Aldrich. LiFePO₄ was bought from Clariant. Polyvinylidene fluoride (PVdF, Solef™ 6010) was purchased from Solvay. Conductive carbon (Shawinigan Black AB50) was provided by Chevron Corp., and high purity lithium metal was purchased by BASF. The LiFePO₄ (LFP) used as cathode active material is a commercial Clariant-LP2.

Preparation of functionalized nanocrystals.—Polyethylene oxide-grafted TiO₂ nanocrystals (PEO_{5K}@TiO₂ NCs) were prepared following the synthesis steps as shown in Fig. 1. The starting reactions were the preparation of TiO₂ nanocrystals covered with oleic acid (OA@TiO₂) (a) and the end-term PO(OH)₂ functionalization of PEO_{5K} (PEO_{5K}-PO(OH)₂) (b). After then, the products a and b were mixed together to allow the ligand-exchange reaction to obtain PEO_{5K}@TiO₂ NCs (c). Full details about synthesis and structural characterization are given in Ref. 20.

Step a—Oleic acid grafted TiO₂.—Oleic acid (OA) was previously degassed at 120 °C for 2 h. It was then cooled down to 90 °C under N₂ flow, and TTIP and 2 M water solution of TMAO were added. The mixture was then heated to 120 °C and then left to react under vigorous stirring for 24 h. The raw product was centrifuged to recover the NCs, which were dispersed in n-hexane or DMC and then precipitated adding ethanol. The OA@TiO₂ NCs were dried in vacuum at 100 °C for one night.

Step b—PEO functionalization with PO(OH)₂.—PEO_{5K} was dissolved in dry DMC and added dropwise to a solution of POCl₃ and TEA in ice bath. The reaction mixture was slowly brought to room temperature and stirred for 24 h. Later that, water was slowly added to the mixture and left to react for 1 h. The solvent was evaporated in vacuum and the raw product was dissolved again in DMC, extracted with acidic water and then extracted three times with saturated brine. The organic phase was collected, dried and precipitated three times with diethyl ether. The PEO_{5K}-PO(OH)₂ was dried in vacuum at 100 °C for one night.

Step c—Ligand exchange process.—PEO_{5K}-PO(OH)₂ and OA@TiO₂ NCs were dispersed in CHCl₃, mixed together, and left to react for 16 h under reflux conditions. The raw product was purified by ultracentrifugation with a mixture of chloroform and diethyl ether with 1:2.5 ratio for at least three times. The PEO_{5K}@TiO₂ NCs were finally dried under primary vacuum at 100 °C for one night.

Characterization of the functionalized nanocrystals.—Both OA@TiO₂ and PEO_{5K}@TiO₂ NCs size was determined by Dynamic Light Scattering (DLS), using a Malvern Zetasizer equipped with a continuous wave 1 mW He–Ne laser operating at 632.8 nm. Thermogravimetric analysis (TGA) was carried out with a Mettler Toledo TGA/DSC1 STARe System. The samples were heated from 25 °C up to 800 °C at 10 °C min⁻¹ in air at constant flow of 50 ml min⁻¹. High resolution ¹H-NMR spectra were

recorded using a Bruker AMX-500 spectrometer operating at 500 MHz, using deuterated chloroform as the solvent.

Preparation of the solid electrolytes PEO_{5K}@TiO₂ NCs/PEO_{4M}/LiTFSI.—The electrolyte membranes were fabricated by standard solvent casting in an argon filled glove box. The proper amounts of PEO_{5K}@TiO₂ NCs, PEO_{4M} and LiTFSI were dissolved in dry acetonitrile or chloroform and slowly stirred for one night. The solutions were poured on PTFE die, left to dry for one night and then the polymer film was detached thanks n-heptane. The membranes were finally dried at room temperature under primary vacuum for one night. In this work, we have explored the membranes composition changing the weight ratio between PEO_{5K}@TiO₂ NCs and PEO_{4M} from 50:50 to 90:10. LiTFSI was added as n = [EO]/[Li] = 10 or 6, where [EO] refers to all the ethylene oxide repeating units in the system. Table I lists the composition of all the prepared samples as determined by TGA measurements (see below).

Characterization of the solid electrolytes.—The thermal properties were investigated by differential scanning calorimetry (DSC) measurements using a Mettler Toledo DSC instrument. The samples were cycled two times from -100 °C up to 150 °C, with heating/cooling rate of 10 °C min⁻¹, under nitrogen gas flow (80 ml min⁻¹).

Solid-state ¹H and ⁷Li NMR spectra were recorded on a 400 MHz Bruker Avance III spectrometer (9.4 T magnet) under static conditions. Attempts to collect MAS spectra at different spinning speeds were performed, but it was not possible to obtain stable and reproducible rotation for all the samples.

¹H one pulse spectra were acquired using 4.5 μs 90° pulse with 6 s of recycle delay and 32 scans with single-pulse sequence. The chemical shift scale was referenced to adamantane as a secondary standard. ⁷Li single pulse spectra were recorded with the use of 2.5 μs 90° pulse with recycle delay of 5 s, 512 scans. The chemical shift scale was referenced to 1 M LiCl solution. ⁷Li spin-lattice relaxation times (T₁) were measured with the use of standard Inversion Recovery pulse sequence. All the spectra were analyzed with the use of DMFit™ and TopSpin™ 3.6 software.

The electrolyte ionic conductivity was measured by Electrochemical Impedance Spectroscopy (Biologic VSP300 equipped with EIS board), in the frequency range from 100 Hz to 1 MHz, and in the temperature range from -20 °C to 80 °C, with 10 mV peak-to-peak signal amplitude. Lithium stripping/plating was performed with a symmetric Li/electrolyte/Li coin cell in galvanostatic conditions using different currents at 70 °C. All the cells were prepared and sealed in glove box filled with Ar (MBraun, [O₂] and [H₂O] < 0.1 ppm).

Preparation and test of the full cell.—LFP-based composite cathodes were prepared by a standard procedure, from a slurry composed of 70 wt% LFP, 20 wt% Shawinigan Black AB50, and 10 wt% PVdF binder in NMP coated on Al, cut into disks of 1.54 cm² and dried under vacuum at 120 °C for 24 h prior to use. Li metal disks (area 1.54 cm²) were cut from a 200 μm thick ribbon. The 50:50 w/w nanocomposite solid electrolyte was sandwiched within the LFP cathode and the Li metal anode (no spacer used) and

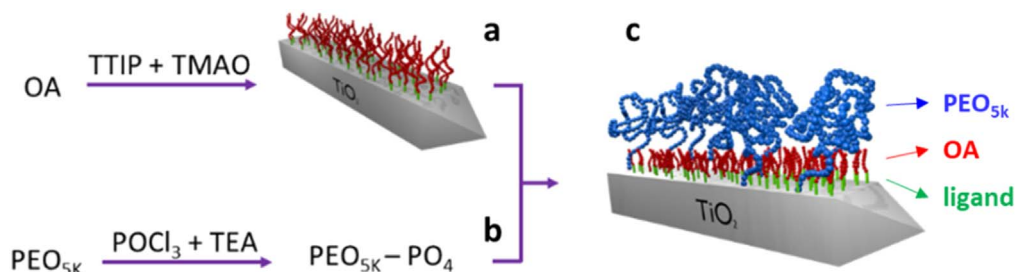


Figure 1. Diagram of synthesis steps: synthesis of OA@TiO₂ (a), PO(OH)₂ functionalization of PEO_{5K} (b), ligand exchange reaction to obtain PEO_{5K}@TiO₂ (c).

Table I. Composition (wt%) of the prepared solid electrolyte samples under study. NC = nanocrystals.

PEO _{5K} @TiO ₂ /PEO _{4M} (w/w)	n = [EO]/[Li]	NC composition (wt%)			PEO _{4M} wt%	PEO tot wt%	LiTFSI wt%
		TiO ₂	OA	PEO _{5K}			
50:50	10:1	18.8	5.8	10.5	35.1	45.6	29.8
70:30	10:1	28.1	8.7	15.8	22.5	38.3	25.0
90:10	10:1	38.7	12.0	21.8	8.1	29.8	19.5
70:30	6:1	34.3	10.7	19.3	7.1	26.4	28.7

assembled into a lab-scale ECC-Std test cell (EL-CELL, Germany), which was stored at 70 °C inside an environmentally controlled chamber MK-20 by BINDER (Germany) for galvanostatic charge/discharge cycling (test carried out on an Arbin BT-2000 battery tester at different current regimes in the potential range 2.8–3.7 V vs Li⁺/Li). Cell assembly was performed inside an Ar-filled dry glovebox (Jacomex GP-concept, O₂ and H₂O content <1 ppm). The charge/discharge cycles were set at the same rate ranging from 0.025 to 0.1 mA. Note that 0.025 mA corresponds to 0.05 C with respect to the LFP active material loading on the electrode of 2.90 mg, viz. $1.85 \pm 0.05 \text{ mg cm}^{-2}$.

Result and Discussion

Physico-chemical properties and composition of the PEO_{5K}@TiO₂ NCs.—Figure 2 shows the DLS characterization of the OA@TiO₂ and PEO_{5K}@TiO₂ NCs (left panel), and the TGA characterization of the PEO_{5K}@TiO₂ NCs (right panel). The DLS panel shows both the raw intensities measured by the instrument (black lines) and the volume data corrected by considering the light scattering correction due to the particles size (red lines). The ligand exchange reaction with PEO determines the increase of the average particle size from ~10.5 nm to ~13 nm.

TGA (Fig. 2, right panel) allowed addressing the actual composition of PEO_{5K}@TiO₂ NCs thanks to the different degradation temperature of PEO and oleic acid. We observe a little mass loss (<3 wt%) below 100 °C, which can be attributed to moisture, and two degradation steps starting at ~170 °C and ~340 °C which are due to the evolution of PEO_{5K} and oleic acid, respectively. After 500 °C there is no further weight variation and the remaining mass is attributed to TiO₂. From TGA, NCs are composed of 53.4 wt% TiO₂, 30% wt% PEO_{5K} and 16.6 wt% oleic acid. The ratio between PEO_{5K} and oleic acid is in agreement with the results of ¹H high resolution NMR (See Supplementary Information, Fig. S1 and related comment is available online at stacks.iop.org/JES/167/070535/mmedia). The thermal properties of the functionalized NCs were also investigated by DSC measurements. Figure S2 shows the DSC thermograms of PEO_{5K}, PEO_{5K}-PO₄, PEO_{5K}@TiO₂.

Physico-chemical properties of the solid electrolyte membranes.—In the following, for the sake of simplicity, the PEO_{5K}@TiO₂ NCs will be shortly called “NC.” Figure 3 shows the DSC thermograms of pure PEO_{4M} and of the prepared electrolytes. PEO_{4M} shows a glass transition, T_g , at -59 °C (see inset), followed by a small feature around -40 °C which can be attributed to the cold crystallization of a small portion of the rubbery phase. A neat melting peak is observed above $T_m = 50$ °C with a melting enthalpy, $\Delta H_m = 134 \text{ Jg}^{-1}$, which corresponds to a crystalline fraction, $X_c \cong 67\%$.²¹ By adding LiTFSI (n = 10) the T_g increases to -51 °C, due to the interactions among the amorphous polymer strands and the Li⁺ ions.¹³ At the same time, the T_m shifts down to ~40 °C with $\Delta H_m = 12,9 \text{ Jg}^{-1}$, which corresponds to a residual crystallinity, $X_c \cong 6\%$. The DSC curves of the nanocomposite electrolyte membranes show the complete disappearance of the PEO melting peak, which means that the NC addition does not allow the polymer strands to reorganize into their typical crystalline helical structure¹³ following solvent evaporation. The glass transition temperature is only marginally affected by the NC addition, ranging between -38 and -35 °C (see inset). In contrast, the increase of salt concentration from n = 10 to n = 6 determines a ~10 °C increase of the T_g to about -28 °C, which is due to stronger interactions among Li⁺ ions and the polymer strands.

Figure 4 shows the ionic conductivity (Arrhenius plots) of PEO_{4M}/LiTFSI, and of the nanocomposite samples with n = EO/Li = 10 and different NC/PEO_{4M} ratio, or with different n = [EO]/[Li] values at constant NC/PEO_{4M} 70:30 ratio. Whereas all the electrolytes display a Vogel-Tammann-Fulcher (VTF) trend,⁶ the PEO_{4M}/LiTFSI shows a clear jump in correspondence of the melting peak revealed by DSC (see Fig. 3). Its conductivity value at 25 °C is in good agreement with that previously reported by our group for the composition n = 8.²² The addition of the nanoparticles determines the progressive decrease of the ionic conductivity, and the disappearance of any jump related to the melting of crystalline phase, in agreement with the DSC results of Fig. 3. Interestingly, the sample with NC/PEO_{4M} ratio of 50:50 shows better conductivity values with respect to the PEO_{4M}/LiTFSI sample below the crystalline phase

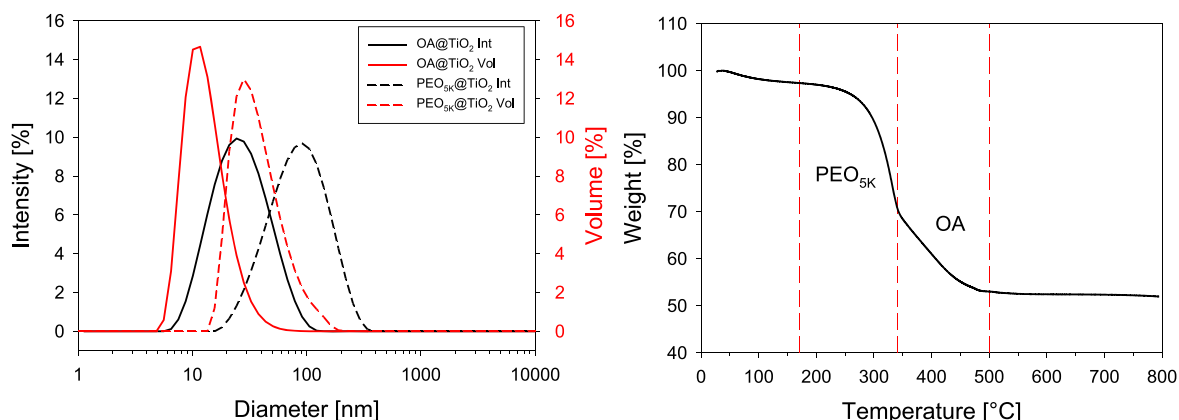


Figure 2. Left panel: DLS measurements of OA@TiO₂ and PEO_{5K}@TiO₂ NCs. The black and red lines represent the raw intensities and the corrected volume results (see text). Right panel: TGA curve of the PEO_{5K}@TiO₂ NCs. The dashed red lines represent the lines of separation between the degradation of PEO and that of oleic acid.

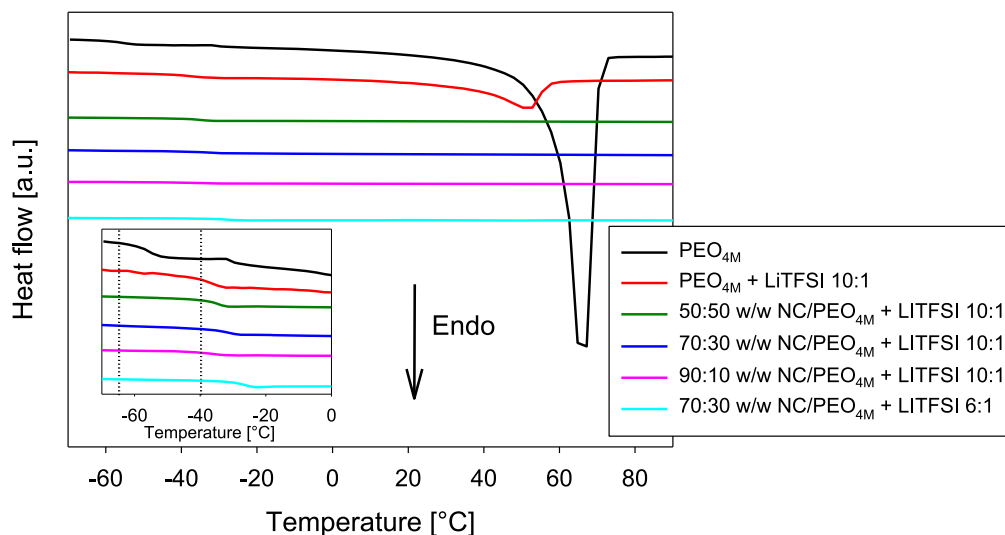


Figure 3. DSC thermograms of the different samples prepared in this work.

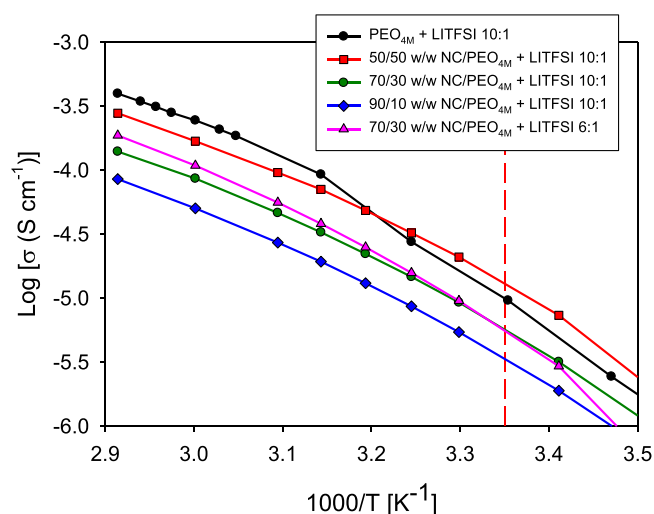


Figure 4. Arrhenius plots of PEO_{4M}/LiTFSI, and of the nanocomposite samples with $n = \text{EO}/\text{Li} = 10$ and different NC/PEO_{4M} ratio, or with different $n = [\text{EO}]/[\text{Li}]$ values at constant NC/PEO_{4M} 70:30 ratio. The dashed red line corresponds to 25 °C.

melting, and its conductivity still exceeds $10^{-4} \text{ S cm}^{-1}$ at 80 °C. Therefore, we selected this sample for further characterization and full cell testing.

Figure 5 shows the ⁷Li stationary solid-state NMR spectra of PEO_{4M}/LiTFSI and of the 50:50 w/w electrolyte membrane, together with their best-fits, whose parameters are reported in Table II. The PEO_{4M}/LiTFSI spectrum can be decomposed in two Lorentzian peaks ($\sim 40:60$ ratio) with Full Width at Half Height (FWHH) which scale of about one order of magnitude. In order to rationalize this linewidth difference, it should be considered that, at the room temperature, PEO-salt systems fall into the motional narrowing regime.²³ In this regime, the correlation times are the order of the Larmor frequency ($\sim 10^{-9} \text{ s}^{-1}$), vs a ⁷Li quadrupolar interaction frequency in the range $10^4\text{--}10^5 \text{ s}^{-1}$. Therefore, the observed residual peak widths are likely due to inhomogeneous broadening and isotropic chemical shift. Other things being equal, the residual peak differences could be related to different mobility. Therefore, we can conclude that the linewidths of the two components scale with cation mobility, as also demonstrated by the Lorentzian shape of both the peaks. The addition of the nanocrystals (sample with NC/PEO_{4M} ratio of 50:50 w/w) determines a $\sim 120\%$ and a $\sim 5\%$

FWHH increase of the more and less mobile populations, respectively, with a 5% variation of the relative intensities. As the conductivity of the 50:50 w/w membrane at r.t. is higher than that of PEO_{4M}/LiTFSI, whereas the FWHHs go in the opposite way, on the basis of the previous discussion we can conclude that the linewidth increase is this time related to a higher matrix disorder due to the filler addition, rather than to a different cation mobility. This is further confirmed by the average T_1 values, which do not change upon nanocrystals addition, at least in the limit of the experimental uncertainty.

Figure 6 shows the stripping/plating test at 70 °C in symmetric Li/electrolyte/Li cells assembled with PEO_{4M}/LiTFSI and with the NC/PEO_{4M} 50:50 w/w electrolyte membranes at different current densities from 50 to 600 $\mu\text{A cm}^{-2}$ (left panel), and the long-term behavior of the latter at 200 $\mu\text{A cm}^{-2}$ (right panel). In the former measurement, ten stripping/plating cycles (0.5 h for stripping and 0.5 h for plating) were applied for each current starting from the lowest value to the highest one. The adopted stripping/plating current regimes are shown in Fig. S3 and used to compare the stability of the two systems in the same conditions. The larger overpotential of the PEO_{4M}/LiTFSI cell (despite its higher conductivity) is due to the different thickness of the casted membranes, i.e. 300 μm vs 100 μm for the PEO_{4M}/LiTFSI and the nanocomposite electrolyte membrane, respectively, which in turn is a direct consequence of the better mechanical properties of the TiO₂-based nanocomposite. Moreover, the PEO_{4M}/LiTFSI cell shows fluctuations in the voltage values at constant current of 100 $\mu\text{A cm}^{-2}$ and the cell is short circuited after few cycles at 200 $\mu\text{A cm}^{-2}$ due to the characteristic dendrite formation. On the contrary, the nanocomposite membrane exhibits better stability, indeed dendrite formation happens at 300 $\mu\text{A cm}^{-2}$, while the cell short circuit takes place after several cycles at 500 $\mu\text{A cm}^{-2}$. We can conclude that large amounts of inorganic nanoparticles inhibit the formation of the filaments and delays the short circuit of the cell, despite the lower thickness of the membrane. To test the long-term stability of the nanocomposite electrolyte, we decided to perform a following stripping/plating measurement by applying the 200 $\mu\text{A cm}^{-2}$ current density up to dendrite formation and cell short circuit, which took place after 245 cycle.

The galvanostatic discharge/charge cycling behavior of the nanocomposite electrolyte with NC/PEO_{4M} 50:50 w/w in Li/electrolyte/LFP cell at 70 °C and at different current regimes is shown in Fig. 7. The electrochemical process of this cell is the reversible removal-uptake of Li⁺ ions to and from the LiFePO₄/FePO₄ active materials,²⁴ which is expected to develop along an average 3.45 V vs Li⁺/Li flat plateau attributed to the insertion/de-insertion process

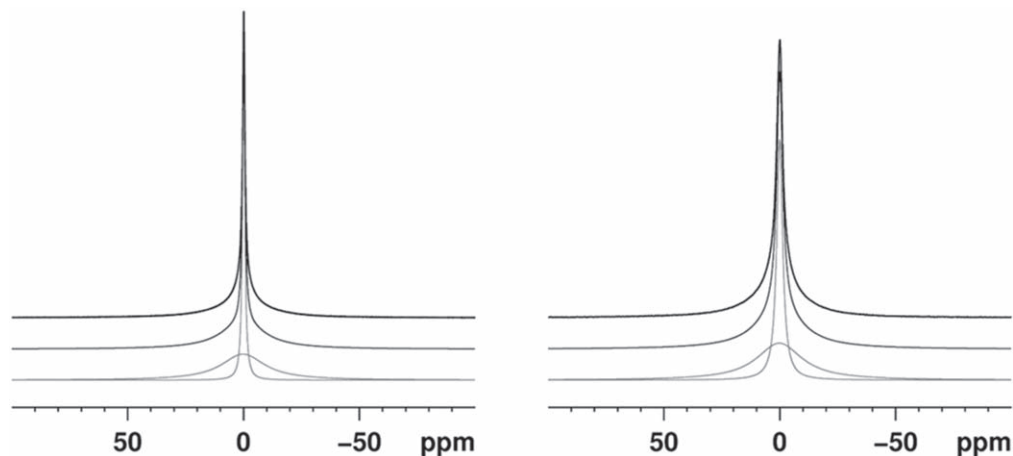


Figure 5. ^7Li stationary solid-state NMR spectra of $\text{PEO}_{4\text{M}}/\text{LiTFSI}$ (left) and the $\text{NC}/\text{PEO}_{4\text{M}}$ 50:50 w/w nanocomposite electrolyte membrane (right), together with their best-fits. From top to bottom: experimental, best-fit, two best-fit components. Best-fits parameters are reported in Table II.

Table II. Best-fit parameters of ^7Li NMR spectra based on a Gaussian/Lorentzian model. FWHH = Full Width at Half Height, Gauss/Lorentz = 0; all the parameters were allowed to vary during the fitting procedure. The longitudinal relaxation times, T_1 , are determined as average values of the two populations.

Sample	Chemical shift (ppm)	FWHH (Hz)	Intensity (%)	T_1 (ms)
$\text{PEO}_{4\text{M}}/\text{LiTFSI}$ 10:1				
Peak 1	-0.01 ± 0.05	221 ± 4	41 ± 1	659 ± 20
Peak 2	0.17 ± 0.05	3524 ± 70	59 ± 1	
50:50 w/w $\text{NC}/\text{PEO}_{4\text{M}}$ + LiTFSI 10:1				
Peak 1	0.00 ± 0.05	483 ± 10	46 ± 1	681 ± 20
Peak 2	0.16 ± 0.05	3700 ± 74	54 ± 1	

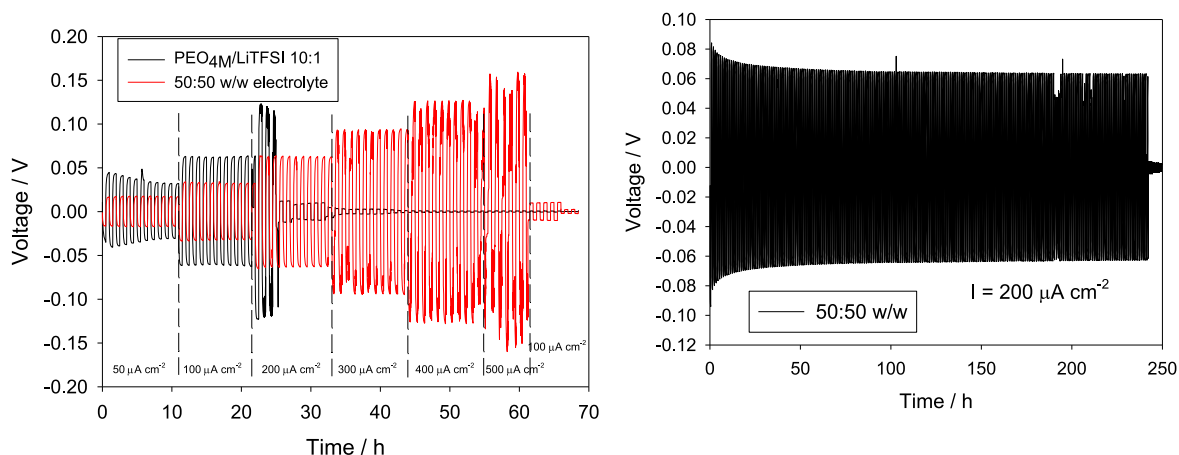


Figure 6. Stripping/plating behavior of $\text{PEO}_{4\text{M}}/\text{LiTFSI}$ and $\text{NC}/\text{PEO}_{4\text{M}}$ 50:50 w/w electrolyte membranes at different working current densities from $50 \mu\text{A cm}^{-2}$ to $500 \mu\text{A cm}^{-2}$ (left panel), and long-term behavior of the 50:50 w/w sample at $200 \mu\text{A cm}^{-2}$ (right panel).

between the octahedral sites of olivine-type phase (see panel A of Fig. 7). The difference between discharge and charge potential values only slightly increased with the increase of the applied current, thus accounting for both sufficiently low internal resistance at the electrode/electrolyte interface and limited cell overpotential contributions. Panel B in Fig. 7 shows the specific capacity vs cycle number at 70°C and different current rates from 0.025 to 0.1 mA, based on the LFP active material mass in the electrode. The initial specific capacity was very low (about 73 mAh g^{-1}) at 0.025 mA (0.05 C); it rapidly increased upon cycling reaching a value exceeding 145 mAh g^{-1} after about 10 cycles, where it stabilized its cycling behavior. This accounts for the system undergoing an activation process in the initial stages, where slowly an increasing portion of the material is activated at the electrochemical reaction.

This phenomenon is most likely due to the slow softening of the solid-state electrolyte at 70°C , which upon time improves the interfacial contact at the electrode/electrolyte interface and the active material wetting, with facilitated lithium ion diffusion and more active sites for reversible reaction with Li^+ ions.

After this activation stage, the capacity retention was satisfactory as well as the rate capability: the cell still delivered specific capacity values exceeding 130 and 120 mAh g^{-1} after 40 and 50 cycles at 0.05 and 0.1 mA, respectively. Thus, the cell operated with the expected potential profiles delivering a high fraction of the theoretical capacity even at higher rates, which is remarkable for a solid polymer composite system. The slight decrease in the specific capacity observed when increasing the current regime can, in general, be ascribed to limitations in the Li^+ ion diffusion in the

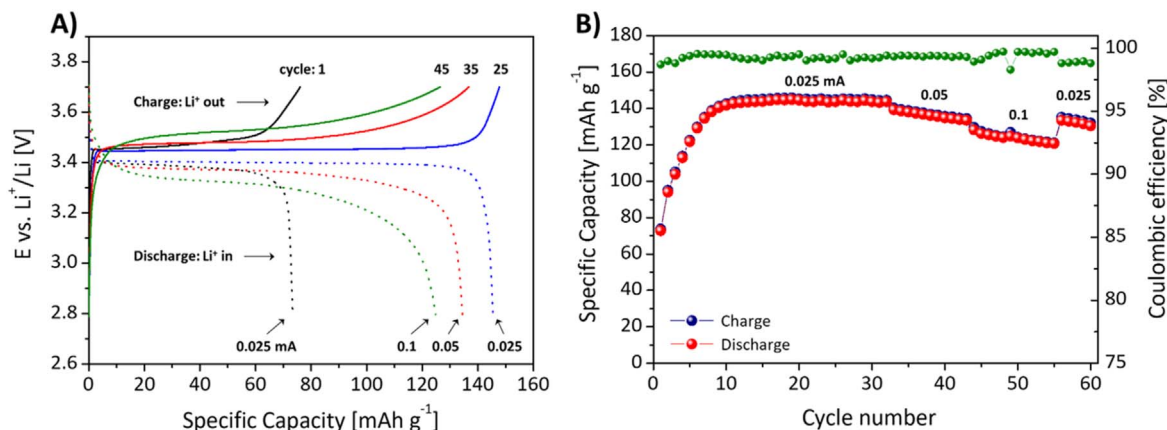


Figure 7. Cycling behavior at 70 °C of the Li/nanocomposite electrolyte/LFP cell at 70 °C and different current regimes (cut-off voltages 2.8–3.7 V vs Li⁺/Li): (a) representative potential vs specific capacity profiles (0.025, 0.05 and 0.1 mA, respectively; note that 0.025 mA corresponds to 0.05 C with respect to the total LFP active material loading on the electrode of 2.90 mg), (b) specific capacity and Coulombic efficiency vs number of cycles.

solid electrolyte, and at the interface with the active material grains. However, the cycling response is also encouraging for a solid system, since the Coulombic efficiency increased to above 99.5% after the initial cycles and, subsequently, remained highly stable throughout the test, indicating excellent reversible cycling after the interface was stabilized. The stability and robustness of the nanocomposite electrolyte-based system after cycling at higher current regimes was confirmed by reducing the current regime from 0.1 to 0.025 mA after the 55th cycle: the cell recovered almost 95% of the specific capacity delivered after 30 cycles.

Conclusions

In this paper, we reported the synthesis and characterization of a polymer-in-ceramic nanocomposite electrolyte encompassing TiO₂ nanocrystals functionalized with low molecular weight PEO ($M_w = 5000$). The blending of this ceramic phase with high molecular weight PEO ($M_w = 4000000$) and LiTFSI ($n = [\text{EO}]/[\text{Li}] = 6, 10$) allowed fabricating solvent-free, solid-state membranes with TiO₂ content as high as ~39 wt%. The membranes were free standing and showed qualitatively good mechanical resistance and dimensional stability. The ionic conductivity displayed a VTF behavior, with values exceeding $10^{-5} \text{ S cm}^{-1}$ at the room temperature, and $3 \times 10^{-4} \text{ S cm}^{-1}$ at 70 °C for the sample 50:50 w/w. Stripping/plating experiments showed an excellent long-term behavior of this composition event at relatively high currents $200 \mu\text{A cm}^{-2}$. The NC/PEO_{4M} 50:50 w/w nanocomposite electrolyte membrane was finally tested in a full Li/electrolyte/LiFePO₄ cell, where it delivered 130 mAh g^{-1} and 120 mAh g^{-1} after 40 and 50 cycles at 0.05 and 0.1 mA, respectively, with Coulombic efficiency higher than 99.5% and remarkable stability upon cycling. Further developments can include the elimination of oleic acid, and the use of active fillers in order to increase the amount of filler which can be added to the polymer matrix without lowering the overall conductivity.

Acknowledgments

Financial support from the Italian Ministry of University and Research (MIUR) through grant “Dipartimenti di Eccellenza 2017—Materials for energy” is gratefully acknowledged. Claudio Gerbaldi gratefully acknowledges the ENABLES project (<http://enables-project.eu/>), which has received funding from the European

Union’s Horizon 2020 research and innovation program, under grant Agreement no. 730957.

ORCID

Michele Mauri  <https://orcid.org/0000-0002-7777-9820>

Piercarlo Mustarelli  <https://orcid.org/0000-0001-9954-5200>

References

- E. Pomerantseva, F. Bonaccorso, X. Feng, Y. Cui, and Y. Gogotsi, *Science*, **366**, eaan8285 (2019).
- https://setis.ec.europa.eu/sites/default/files/set_plan_batteries_implementation_-_plan.pdf.
- P. Albertus, S. Babinec, S. Litzelman, and A. Newman, *Nat. Energy*, **3**, 16 (2018).
- P. G. Bruce, S. A. Freunberger, L. J. Hardwick, and J. M. Tarascon, *Nat. Mater.*, **11**, 19 (2012).
- E. Quartarone and P. Mustarelli, *J. Electrochem. Soc.*, **167**, 050508 (2020).
- E. Quartarone and P. Mustarelli, *Chem. Soc. Rev.*, **40**, 2525 (2011).
- B. Liu, J.-G. Zhang, and W. Xu, *Joule*, **2**, 833 (2018).
- M. D. Tikekar, S. Choudhury, Z. Tu, and L. A. Archer, *Nat. Energy*, **1**, 16114 (2016).
- Y. Wang, W. D. Richards, S. P. Ong, L. J. Miara, J. C. Kim, Y. Mo, and G. Ceder, *Nat. Mater.*, **14**, 1026 (2015).
- M. Keller, G. B. Appetecchi, G.-T. Kim, V. Sharova, M. Schneider, J. Schuhmacher, A. A. Roters, and S. Passerini, *J. Power Sources*, **353**, 287 (2017).
- J. C. Bachman et al., *Chem. Rev.*, **116**, 140 (2016).
- A. Manthiram, X. Yu, and S. Wang, *Nat. Rev. Mater.*, **2**, 16103 (2017).
- E. Quartarone, P. Mustarelli, and A. Magistris, *Solid State Ionics*, **110**, 1 (1998).
- L. Fan, S. Wei, S. Li, Q. Li, and Y. Lu, *Adv. Energy Mater.*, **8**, 1702657 (2018).
- L. Chen, Y. Li, S. Li, L. Fan, C. Nan, and J. B. Goodenough, *Nano Energy*, **46**, 176 (2018).
- M. Keller, A. Varzi, and S. Passerini, *J. Power Sources*, **392**, 206 (2018).
- D. Li, L. Chen, T. Wang, and L. Fan, *ACS Appl. Mater. Interfaces*, **10**, 7069 (2018).
- S. Bonizzoni, C. Ferrara, V. Berbenni, U. Anselmi-Tamburini, P. Mustarelli, and C. Tealdi, *PCCP*, **21**, 6142 (2019).
- G. Piana, F. Bella, F. Geobaldo, G. Meligrana, and C. Gerbaldi, *Journal of Energy Storage*, **26**, 100947 (2019).
- D. Selli, M. Tawfilas, M. Mauri, R. Simonutti, and C. Di Valentin, *Chem. Mater.*, **31**, 7531 (2019).
- A. Magistris, P. Mustarelli, E. Quartarone, and C. Tomasi, *Solid State Ionics*, **136–137**, 1241 (2000).
- C. Capiglia, P. Mustarelli, E. Quartarone, C. Tomasi, and A. Magistris, *Solid State Ionics*, **118**, 73 (1999).
- P. Mustarelli, C. Capiglia, E. Quartarone, C. Tomasi, P. Ferloni, and L. Linati, *Phys. Rev. B*, **60**, 7228 (1999).
- G. Meligrana, C. Gerbaldi, A. Tuel, S. Bodoardo, and N. N. Penazzi, *J. Power Sources*, **160**, 516 (2006).